Linear Elastic Fracture Mechanics Approach to Plate End Debonding in Rectilinear and Curved Plated Beams

L. De Lorenzis[1,*], M. Paggi[2], A. Carpinteri[2] and G. Zavarise[1]

[1]University of Salento, Department of Innovation Engineering Via per Monteroni, 73100 Lecce, Italy
[2]Politecnico di Torino, Department of Structural and Geotechnical Engineering C.so Duca degli Abruzzi 24, 10129 Torino, Italy

Abstract: This paper proposes a linear elastic fracture mechanics approach for the prediction of plate end debonding in rectilinear and curved plated beams. The analytical model results in simple equations, suitable for immediate design use. The load-deflection curve of a plated beam, from the onset of debonding up to the complete separation of the plate, is obtained by controlling the length of the interfacial debonding crack. Its shape clearly shows that snap-back or snap-through instabilities may arise when the beam is loaded under displacement or force control. Analytical predictions are also compared with finite element results based on an interfacial cohesive crack model. It is shown that the predictions of the proposed analytical model match closely the numerical solution, provided that an effective crack length accounting for the size of the fracture process zone is used in the calculations.

Key words: curved beams, plate end debonding, finite elements, fracture mechanics, FRP reinforcement, plated beams, snap-back instability.

1. INTRODUCTION

Plate bonding is an effective and cost-efficient technique to increase the load-bearing capacity and/or the stiffness of existing beams. In the past decade, fiber-reinforced polymer (FRP) composite plates have almost totally replaced the more traditional steel plates for this application. Among the possible failure modes of plate bonded beams, several mechanisms related to debonding of the plate from the substrate have been identified by previous researchers. Due to the brittle and unstable character of such failures, their prediction has been the subject of several investigations. In particular, this paper focuses on the so-called "plate end debonding" mechanism, whereby failure occurs by the formation and rapid growth of an interfacial crack between the end of the plate and the beam.

A detailed review of existing models for prediction of plate end debonding failures is available in Smith and Teng (2002). Most of the models reviewed therein adopt a stress-based criterion for failure prediction. Rabinovitch and Frostig (2001) proposed a fracture-mechanics based approach, where the higher-order theory is used for the stress analysis of the plated beam, and the J-integral formulation is adopted for the evaluation of the energy release rate. In the attempt to simplify the formulation, Rabinovitch (2004) adopted the virtual crack extension method coupled with different stress analysis models, including: (i) the two- and one-parameter elastic foundation models for the evaluation of the interfacial stresses between the plate and the substrate, (ii) the equivalent beam model, (iii) the finite element analysis. By comparing results

*Corresponding author. Email address: laura.delorenzis@unisalento.it; Fax: +39-0832-325362; Tel: +39-0832-297241.

with those obtained from the application of the higher-order theory, he showed that the virtual crack extension method using the stress results of the elastic foundation models provides an acceptable estimate of the energy release rate.

In the most recent studies on plate end debonding, fracture mechanics based approaches are becoming increasingly established (Colombi 2006; Carpinteri *et al.* 2007c). Carpinteri *et al.* (2007c) used a three-dimensional finite element model to analyze plate end debonding in beams with non-rectangular cross-section, assuming a linear behaviour for the materials and a non-linear interfacial cohesive law for the plate-substrate interface. Their results show that, when the bending stiffness of the plated beam is considerably higher than that of the unplated beam, snap-back instabilities may take place.

In this paper, a linear elastic fracture mechanics approach is proposed for the prediction of plate end debonding in rectilinear and curved plated beams. This approach is analogous to the equivalent beam model adopted by Rabinovitch (2004) and aims at simplifying more detailed models based on the elastic foundation theory (Carpinteri *et al.* 2007a; Carpinteri *et al.* 2009a; Cornetti *et al.* 2007). Useful closed-form solutions to estimate the critical load for the onset of plate end debonding are herein determined. Moreover, the analysis is extended to the determination of the entire load–deflection curve of the beam, obtained according to a crack length control scheme, as first proposed by Carpinteri (1985, 1989) for the study of crack propagation into homogeneous materials and then recently generalized to interface mechanical problems by Carpinteri *et al.* (2005). The shape of the obtained curves delivers interesting information on the beam behaviour during the whole process of plate end debonding, and on the role played by the most significant design variables. Finally, analytical predictions are compared with the results of a nonlinear finite element model. This model assumes linearly elastic behaviour for the materials, but considers a nonlinear interface cohesive law taking into account Mixed Mode effects (Carpinteri and Paggi 2008; Carpinteri and Paggi 2010). Predictions provided by the analytical model are expected to deviate quite significantly from those obtained on the basis of a more sophisticated approach, in accordance with previous results (Rabinovitch 2004). However, it is shown that a suitably enhanced version of the analytical model can be devised to match more closely the numerical solution.

2. MODELING ASSUMPTIONS

The model is based on the following assumptions:

- plane cross-sections remain plane for both the unstrengthened (unplated) and the strengthened (plated) portions of the beam;
- beam and plate materials are assumed to be linearly elastic;
- the gradual development of composite action between the beam and the strengthening plate is neglected. Hence, all sections in presence of a bonded plate have bending stiffness EI_s, whereas all unplated sections have stiffness EI_u. This corresponds to assuming an infinite stiffness of the curve giving the interfacial shear stress, p_T, versus the tangential relative displacement, g_T, which is coherent with the use of linear elastic fracture mechanics;
- for the symmetric load scheme of Figure 1, the interfacial crack of length a develops symmetrically at the plate ends on both sides of the beam and propagates always in the same

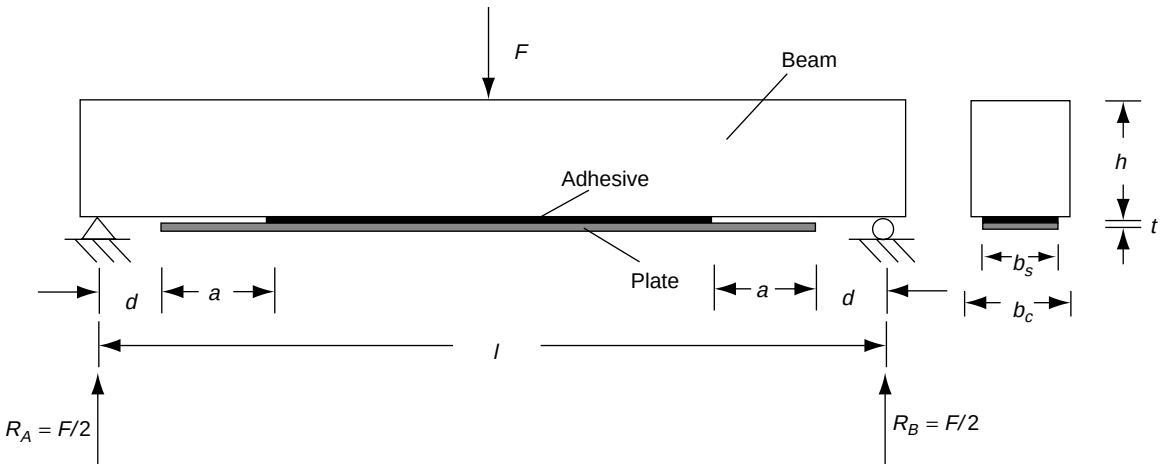

Figure 1. Rectilinear plated beam under a mid-span force

direction. In other words, the crack is assumed to propagate in pure Mode II conditions, i.e. Mixed Mode effects are neglected. For the sake of simplicity, Figure 1 shows that the crack forms in the adhesive. Its actual path follows the weakest link between the substrate, the adhesive, the interface between substrate and adhesive, and the interface between adhesive and plate.

3. ANALYTICAL MODEL – RECTILINEAR BEAMS

The model considers a simply supported plated beam of length l, loaded with a point load F at the mid-span (see Figure 1).

3.1. Mid-Span Deflection and Compliance

Using elementary structural mechanics (Timoshenko and Young 1965), it can be easily shown that the mid-span deflection of the beam under three-point bending is given by

$$v = F\left[\frac{l^3}{48EI_s} + \frac{(d+a)^3}{6}\left(\frac{1}{EI_u} - \frac{1}{EI_s}\right)\right] \tag{1}$$

where d is the distance between the support and the cutoff section of the strengthening plate, and a is the length of the interfacial crack. Hence, the compliance C is a function of a, and can be expressed as

$$C(a) = \frac{v}{F} = \frac{l^3}{48EI_s} + \frac{(d+a)^3}{6}\left(\frac{1}{EI_u} - \frac{1}{EI_s}\right) \tag{2}$$

As it is reasonable to expect, the compliance increases with the length of the interfacial crack. Considering the whole range $0 \le a \le (l/2 - d)$, the compliance varies between a minimum value, $C_{\min}$, and a maximum value, $C_{\max}$:

$$C_{\min} = C(0) = \frac{l^3}{48EI_s} + \frac{d^3}{6}\left(\frac{1}{EI_u} - \frac{1}{EI_s}\right) \tag{3a}$$

$$C_{\max} = \frac{l^3}{48EI_s} + \frac{(l/2)^3}{6}\left(\frac{1}{EI_u} - \frac{1}{EI_s}\right) = \frac{l^3}{48EI_u} \tag{3b}$$

where $C_{\max}$ corresponds to the compliance of the unplated beam.

3.2. Energy Release Rate and Conditions for Crack Propagation

Under load control, the energy release rate is given by a basic expression of linear elastic fracture mechanics (Anderson 1994) as

$$G = \frac{F^2}{4b_s}\frac{dC}{da}\bigg|_F \tag{4}$$

where b_s is the width of the plate. Combining the derivative of Eqn 2 with Eqn 4 yields

$$G = \frac{F^2}{8b_f}(d+a)^2\left(\frac{1}{EI_u} - \frac{1}{EI_s}\right) \tag{5}$$

The value of the applied load leading to crack propagation in presence of an interfacial crack of length a, $F_{cr}(a)$, can be obtained by equating the energy release rate given by Eqn 5 to its critical value, G_{cr}. Note that, following the assumptions of the model, this critical value corresponds to the interfacial fracture energy in Mode II. The resulting expression for the critical load is

$$F_{cr}(a) = \sqrt{\frac{8b_f G_{cr}}{(d+a)^2\left(\frac{1}{EI_u} - \frac{1}{EI_s}\right)}} \tag{6}$$

Under displacement control, the energy release rate is again given by a basic expression of linear elastic fracture mechanics (Anderson 1994) as

$$G = \frac{v^2}{4C^2 b_f}\frac{dC}{da}\bigg|_v \tag{7}$$

which yields

$$G = \frac{v^2}{8b_f}\frac{(d+a)^2\left(\frac{1}{EI_u} - \frac{1}{EI_s}\right)}{\left[\frac{l^3}{48EI_s} + \frac{(d+a)^3}{6}\left(\frac{1}{EI_u} - \frac{1}{EI_s}\right)\right]^2} \tag{8}$$

Note that Eqn 8 can also be obtained by combining Eqns 1 and 5. The value of the applied mid-span deflection leading to crack propagation in presence of an interfacial crack of length a, $v_{cr}(a)$, can be obtained by equating the energy release rate given by Eqn 8 to its critical value, G_{cr}. It can also be expressed as follows

$$v_{cr}(a) = C(a)F_{cr}(a) \tag{9}$$

where $C(a)$ and $F_{cr}(a)$ are given by Eqns 2 and 6, respectively.

3.3. Dimensionless Formulation

It is now assumed that the beam cross-section is rectangular, of width b_c and depth h. The plate has width b_s and thickness t, and E_c and E_s are, respectively, the elastic moduli of the beam material and of the strengthening plate. A few dimensionless variables are now introduced: the dimensionless beam depth $\bar{h} = h/l$, the dimensionless plate width $\bar{b}_s = b_s/b_c$, and the dimensionless plate thickness $\bar{t} = t/h$. An elastic analysis of the cross-section shows that, in the particular case of $\bar{b}_s = 1$, the bending stiffness ratio between plated and unplated cross-sections is given by

$$k = \frac{EI_s}{EI_u} = \frac{n^2\bar{t}^4 + 4n\bar{t}^3 + 6n\bar{t}^2 + 4n\bar{t} + 1}{n\bar{t} + 1} \tag{10}$$

where $n = E_s/E_c$ is the modular ratio between plate and beam materials. By introducing the dimensionless crack length $\bar{a} = a/l$, and the dimensionless distance between the support and the cutoff section of the strengthening plate, $\bar{d} = d/l$, and with simple manipulations, Eqn 6 can be cast in dimensionless form as follows

$$\bar{F}_{cr}\left(\bar{a}\right) = \frac{F_{cr}\left(a\right)}{b_s\sqrt{EG_{cr}h}} = \sqrt{\frac{2}{3}\frac{\bar{h}^2}{\bar{b}_s\left(\bar{a}+\bar{d}\right)^2}\frac{k}{k-1}} \tag{11}$$

and Eqn 2 in dimensionless form becomes

$$\bar{C}\left(\bar{a}\right) = C\left(a\right)\frac{b_s\sqrt{EG_{cr}h}}{l} = \frac{\bar{b}_s\sqrt{\bar{G}_{cr}}}{4k\bar{h}^2}\left[1+8\left(k-1\right)\left(\bar{a}+\bar{d}\right)^3\right] \tag{12}$$

In the previous equations, the dimensionless critical force $\bar{F}_{cr}$ and the dimensionless compliance $\bar{C}$ have been introduced. Also, the dimensionless Mode II fracture energy has been defined as $\bar{G}_{cr} = G_{cr}/Eh$. Finally, from Eqns 11 and 12, the following dimensionless version of Eqn 9 is easily found

$$\bar{v}_{cr}(\bar{a}) = \bar{C}(\bar{a})\bar{F}_{cr}(\bar{a}) \tag{13}$$

where $\bar{v}_{cr} = v_{cr}/l$ is the dimensionless critical mid-span deflection.

3.4. Load-Displacement Relationship

The previous simple analysis allows to follow the entire load vs. mid-span displacement relationship of the strengthened beam. Assuming that the initial length of the interfacial crack is zero, no propagation occurs until $F_{cr}(0)$ and $v_{cr}(0)$ (given by Eqns 6 and 9 with $a = 0$, respectively) are reached. In this stage, the load-deflection response of the beam is linear with compliance given by Eqn 3(a). The subsequent load-displacement response can be obtained by combining $F_{cr}(a)$ and $v_{cr}(a)$ given by Eqns 6 and 9, or, using the dimensionless form, by combining $\bar{F}_{cr}(\bar{a})$ and $\bar{v}_{cr}(\bar{a})$ given by Eqns 11 and 13.

4. ANALYTICAL MODEL – CURVED BEAMS

A scheme of a plated curved beam is shown in Figure 2. For the sake of simplicity, we assume that the radius of curvature is constant along the span of the beam, and is much larger than the cross-sectional dimensions. Both assumptions are usually valid for civil engineering structures. The beam is simply supported, and is loaded with a point load F at mid-span. The symbols adopted in the following are defined in Figure 2. The position coordinate is the angle α, measured clockwise from the horizontal line; r is the radius of curvature of the mid-adhesive axis; and y_1 is the distance from the bottom of the unplated beam to its centroid, i.e. half of the depth of the unplated beam. According to Figure 2, the beam span l, measured between the extreme points of the centroidal axis of the unplated beam, can be related to the angle α_0, which identifies the initial section of the beam, through simple geometrical considerations. Similarly, the angle α_d, which identifies the initial section of the strengthening plate, can be related to the curvilinear distance from the end of the plate to the end of the beam soffit, d_r, or, equivalently, to the distance Δx_d. Finally, the angle α_a, identifying the tip of the debonding crack, can be expressed in terms of the interfacial curvilinear crack length a. The corresponding relationships are:

$$l = 2\left(r + y_1\right)\cos\alpha_0 \tag{14a}$$

$$d_r = r\left(\alpha_d - \alpha_0\right) \tag{14b}$$

$$\Delta x_d = \frac{l}{2} - r\cos\alpha_d \tag{14c}$$

$$\alpha_a = \alpha_d + \frac{a}{r} \tag{14d}$$

4.1. Mid-Span Deflection and Compliance

The normal force, N, and the bending moment, M, along half of the beam (exploiting symmetry) can be easily expressed as follows:

$$\left.\begin{aligned} N(\alpha) &= \frac{F}{2}\cos\alpha \\ M(\alpha) &= \frac{F}{2}\left(r + y_1\right)\left(\cos\alpha_0 - \cos\alpha\right) \end{aligned}\right\} \quad \alpha_0 \le \alpha \le \frac{\pi}{2} \tag{15}$$

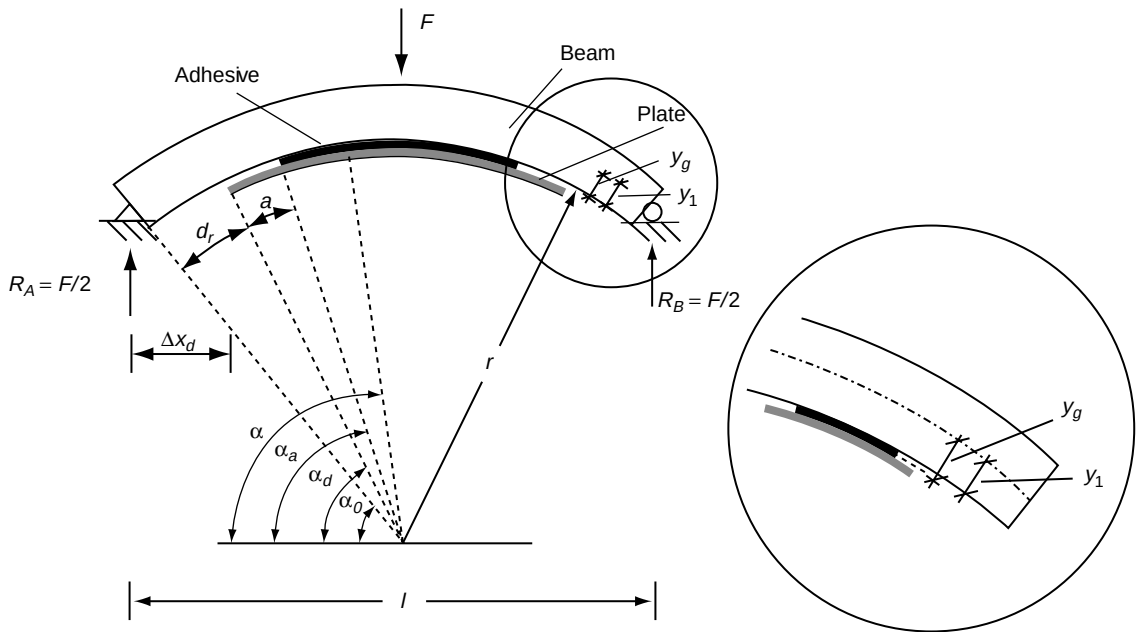

Figure 2. Curved plated beam under a mid-span force

Note that, in writing the above equations, the small difference between y_1 and y_g, the latter being the distance of the centroid of the plated cross-section from the mid-adhesive axis, has been neglected. Using the principle of virtual work (Timoshenko and Young 1965), the mid-span deflection can be expressed as follows:

$$v = \frac{2}{F}\left\{\int_{\alpha_0}^{\alpha_a}\left[\frac{N^2(\alpha)}{EA_u}+\frac{M^2(\alpha)}{EI_u}\right](r+y_1)\,d\alpha + \int_{\alpha_a}^{\pi/2}\left[\frac{N^2(\alpha)}{EA_s}+\frac{M^2(\alpha)}{EI_s}\right](r+y_1)\,d\alpha\right\} \tag{16}$$

where EA_u and EA_s denote the axial stiffnesses of the unstrengthened and strengthened cross-sections, respectively. Integration leads to the following expression for the compliance C:

$$C(\alpha_a) = \frac{v}{F} = \frac{r+y_1}{8}\left[\frac{2\alpha_a+\sin 2\alpha_a-2\alpha_0-\sin 2\alpha_0}{EA_u}+\frac{\pi-2\alpha_a-\sin 2\alpha_a}{EA_s}\right]+ \frac{(r+y_1)^3}{2}\cdot\left[\frac{\cos^2\alpha_0(\alpha_a-\alpha_0)+\frac{1}{2}(\alpha_a-\alpha_0)+\frac{1}{4}(\sin 2\alpha_a-\sin 2\alpha_0)-2\cos\alpha_0(\sin\alpha_a-\sin\alpha_0)}{EI_u}+ +\frac{\cos^2\alpha_0\left(\frac{\pi}{2}-\alpha_a\right)+\frac{1}{2}\left(\frac{\pi}{2}-\alpha_a\right)-\frac{1}{4}\sin 2\alpha_a-2\cos\alpha_0(1-\sin\alpha_a)}{EI_s}\right] \tag{17}$$

where the dependence on a is built into angle α_a, given by Eqn 14(d). As it is reasonable to expect, the compliance increases with the length of the interfacial crack. Considering that $\alpha_d \le \alpha_a \le \pi/2$, it follows that C varies between a minimum value, $C_{\min} = C(\alpha_d)$, which can be obtained from Eqn 17 by replacing α_a with α_d, and a maximum value, $C_{\max}$, corresponding to the compliance of the unplated beam, obtained from Eqn 17 for $\alpha_a = \frac{\pi}{2}$:

$$C_{\max} = C\left(\frac{\pi}{2}\right) = \frac{r+y_1}{8}\left[\frac{\pi-2\alpha_0-\sin 2\alpha_0}{EA_u}\right] + \frac{(r+y_1)^3}{2EI_u}\left[\left(\cos^2\alpha_0+\frac{1}{2}\right)\left(\frac{\pi}{2}-\alpha_0\right) + \frac{\cos\alpha_0}{2}(3\sin\alpha_0-4)\right] \tag{18}$$

4.2. Energy Release Rate and Conditions for Crack Propagation

In load control, the energy release rate is still given by Eqn 4. Computing $dC/d\alpha_a$ from Eqn 17 and noting that from Eqn 14(d) it is $d\alpha_a/da = 1/r$, it is straightforward to compute dC/da. Combining this with Eqn 4 yields:

$$G = \frac{F^2}{4b_s}\left[f_A(r,\alpha_a)\left(\frac{1}{EA_u} - \frac{1}{EA_s}\right) + f_I(r,\alpha_a)\left(\frac{1}{EI_u} - \frac{1}{EI_s}\right)\right] \tag{19}$$

where:

$$f_A(r,\alpha_a) = \frac{r+y_1}{2r}\cos^2\alpha_a \tag{20a}$$

$$f_I(r,\alpha_a) = \frac{(r+y_1)^3}{2r}(\cos\alpha_0 - \cos\alpha_a)^2 \tag{20b}$$

The value of the load leading to crack propagation in presence of an interfacial crack of length a can be obtained by equating the energy release rate given by Eqn 19 to its critical value, G_{cr}:

$$F_{cr}(\alpha_a) = \sqrt{\frac{4b_s G_{cr}}{f_A(r,\alpha_a)\left(\frac{1}{EA_u} - \frac{1}{EA_s}\right) + f_I(r,\alpha_a)\left(\frac{1}{EI_u} - \frac{1}{EI_s}\right)}} \tag{21}$$

where, as usual, the dependence on a is built into angle α_a. In particular, if the initial length of the crack is equal to zero, we have:

$$F_{cr}(a=0) = F_{cr}(\alpha_a = \alpha_d) = \sqrt{\frac{4b_s G_{cr}}{f_A(r,\alpha_d)\left(\frac{1}{EA_u} - \frac{1}{EA_s}\right) + f_I(r,\alpha_d)\left(\frac{1}{EI_u} - \frac{1}{EI_s}\right)}} \tag{22}$$

where $f_A(r, \alpha_d)$ and $f_I(r, \alpha_d)$ can be obtained from Eqns 20(a) and 20(b) by substituting α_a with α_d. Once F_{cr} is reached, the crack propagation progresses unstably. Under displacement control, the energy release rate is still given by Eqn 7. From the definition of compliance in Eqn 2, written in the critical state, the value of the applied displacement leading to crack propagation in presence of an interfacial crack of length a can be expressed as follows:

$$v_{cr}(\alpha_a) = C(\alpha_a)F_{cr}(\alpha_a) \tag{23}$$

where $C(\alpha_a)$ and $F_{cr}(\alpha_a)$ are given by Eqns 17 and 21, respectively. In particular, if the initial length of the crack is equal to zero, we have $\alpha_a = \alpha_d$. Once v_{cr} is reached, the crack propagation progresses stably.

4.3. Dimensionless Formulation

As for rectilinear beams, it is now assumed that the beam cross-section is rectangular and the same symbols previously introduced are used. With simple manipulations, Eqn 21 can be cast in dimensionless form as follows:

$$\begin{aligned}\overline{F}_{cr}(\alpha_a) &= \frac{F_{cr}(\alpha_a)}{b_s\sqrt{EG_{cr}h}} \\ &= 4\left\{\overline{b}_s\left(2+\frac{\overline{h}}{\overline{r}}\right)\left[\cos^2\alpha_a\frac{k_A-1}{k_A} + 3\left(\frac{2\overline{r}}{\overline{h}}+1\right)^2 (\cos\alpha_0 - \cos\alpha_a)^2\frac{k-1}{k}\right]\right\}^{-1/2}\end{aligned} \tag{24}$$

where $\overline{r} = r/l$ is the dimensionless radius of curvature and $k_A = EA_s/EA_u$ is the axial stiffness ratio between plated and unplated cross-sections. Note that $\frac{1-\overline{h}}{2} \le \overline{r} < +\infty$, where the lower value corresponds to the semicircular beam, and the upper limit corresponds to the rectilinear beam. Elastic analysis of the cross-section easily shows that, in the particular case of $\overline{b}_s = 1$, we have $k_A = 1 + n\overline{t}$. Moreover, Eqn 17 can be cast in dimensionless form as

$$\begin{aligned}\overline{C}(\alpha_a) = C(\alpha_a)\frac{b_s\sqrt{EG_{cr}h}}{l} = \frac{\overline{b}_s\overline{h}\sqrt{\overline{G}_{cr}}}{8}\left(\frac{\overline{r}}{\overline{h}}+\frac{1}{2}\right)\Bigg\{\Bigg[2\alpha_a + \sin 2\alpha_a - 2\alpha_0 - \sin 2\alpha_0 + \frac{1}{k_A}(\pi - 2\alpha_a - \sin 2\alpha_a)\Bigg] + \\ +48\left(\frac{\overline{r}}{\overline{h}}+\frac{1}{2}\right)^2\Bigg[\cos^2\alpha_0(\alpha_a-\alpha_0) + \frac{1}{2}(\alpha_a-\alpha_0) + \frac{1}{4}(\sin 2\alpha_a - \sin 2\alpha_0) - 2\cos\alpha_0(\sin\alpha_a - \sin\alpha_0) + \\ +\frac{1}{k}\left(\cos^2\alpha_0\left(\frac{\pi}{2}-\alpha_a\right) + \frac{1}{2}\left(\frac{\pi}{2}-\alpha_a\right) - \frac{1}{4}\sin 2\alpha_a - 2\cos\alpha_0(1-\sin\alpha_a)\right)\Bigg]\Bigg\}\end{aligned} \tag{25}$$

Finally, from Eqns 24 and 25 the following dimensionless version of Eqn 23 is easily found:

$$\bar{v}_{cr}(\alpha_a) = \bar{C}(\alpha_a)\bar{F}_{cr}(\alpha_a) \tag{26}$$

4.4. Load-Displacement Relationship

Also in this case, the previous simple analysis allows to follow the entire load vs. mid-span displacement relationship of the strengthened beam. Assuming that the initial length of the interfacial crack is zero, no propagation occurs until $F_{cr}(\alpha_d)$ and $v_{cr}(\alpha_d)$ are reached. In this phase, the load-displacement behavior of the beam is linear with compliance given by $C(\alpha_d)$ in Eqn 17. The load – displacement behavior after the first propagation of the interfacial crack can be obtained by combining $F_{cr}(\alpha_a)$ and $v_{cr}(\alpha_a)$ given by Eqns 21 and 23 or, in dimensionless form, by combining $\bar{F}_{cr}(\alpha_a)$ and $\bar{v}_{cr}(\alpha_a)$ given by Eqns 24 and 26.

5. FINITE ELEMENT MODEL

In the two-dimensional finite element (FE) model of the plated beam, plane stress eight-node finite elements are used for the discretization of the continuum. Two finite element meshes for a rectilinear and a curved plated beam are shown in Figure 3. As the study mainly focuses on the onset and stability of the plate end debonding process, and in accordance with the assumptions of the analytical model, the beam and plate materials are both assumed linearly elastic. The non-linear behaviour is then located at the interface. This assumption, while preventing a direct comparison of the model predictions with test results, allows to concentrate the analysis on the non-linearities related to the interface, and thus to isolate the effects of the debonding process from those of the other non-linear phenomena. On the other hand, when thick plates are bonded to concrete beams, the onset of debonding may occur at low load levels, at which the global behavior of the beam is still close to linearity.

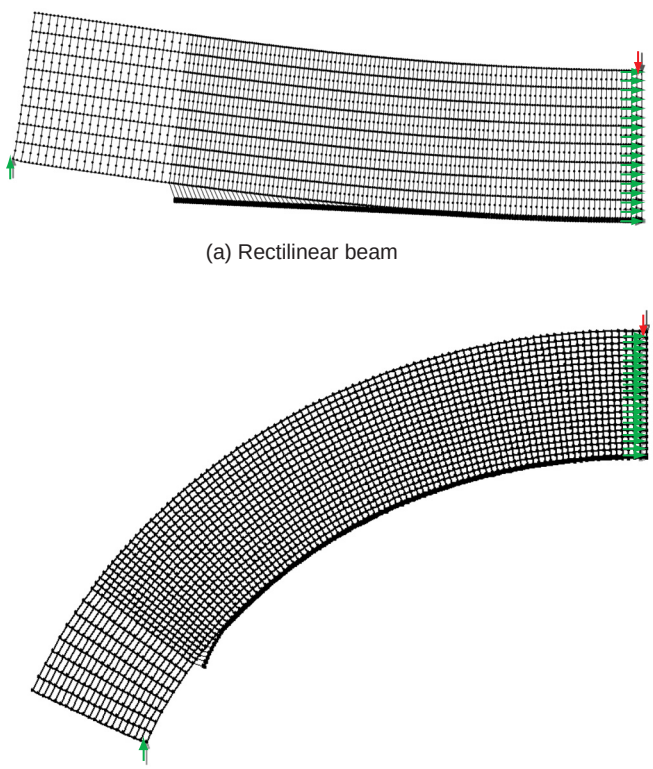

(a) Rectilinear beam

(b) Curved beam

Figure 3. Deformed FE mesh during the plate end debonding process (magnification = 50)

The plate-substrate interface is modelled with zero-thickness interface elements. The mechanical behaviour of such elements is usually described by suitable interface constitutive laws, where the equivalent nodal forces transmitted along the interface are related to the displacement discontinuities in the corresponding directions (see also Paggi *et al.* 2006, for a detailed overview of interface constitutive laws). The plate-substrate interface in the problem under examination is subjected to both shear and normal stresses, hence interfacial constitutive laws have to be assumed in both directions. For a review of different possible approaches in cohesive zone modelling of Mixed Mode fracture problems, see De Lorenzis and Zavarise (2008).

In the present paper, coupled cohesive laws derived from a potential are considered in the normal and tangential directions. With this approach, the fracture energy is the same in all mode mixities. The Mode I cohesive law relates the normal relative displacement, $g_N > 0$, to the normal stress, p_N, while the Mode II law relates the tangential relative displacement, g_T, to the tangential stress, p_T. Frequently used coupled cohesive laws derived from a potential are those developed in Tvergaard (1990) and Tvergaard and Hutchinson (1992). Both use a dimensionless coupling parameter between the normal and tangential laws. The present study adopts a simplified version of the laws in Tvergaard and Hutchinson (1992), where the constant branch of the curves is taken of zero length. Hence, the cohesive laws implemented herein are bilinear (Figure 4). This simple shape is able to capture the three characteristic parameters of the interface, i.e. the fracture energies (areas underneath the curves), the cohesive strengths, $p_{N\max}$ and $p_{T\max}$, and the linear elastic properties (slopes of the curves in the ascending branch). For this reason the bilinear model is often used to model the interfacial behaviour of FRP bonded to quasi-brittle substrates (Yuan *et al.* 2004).

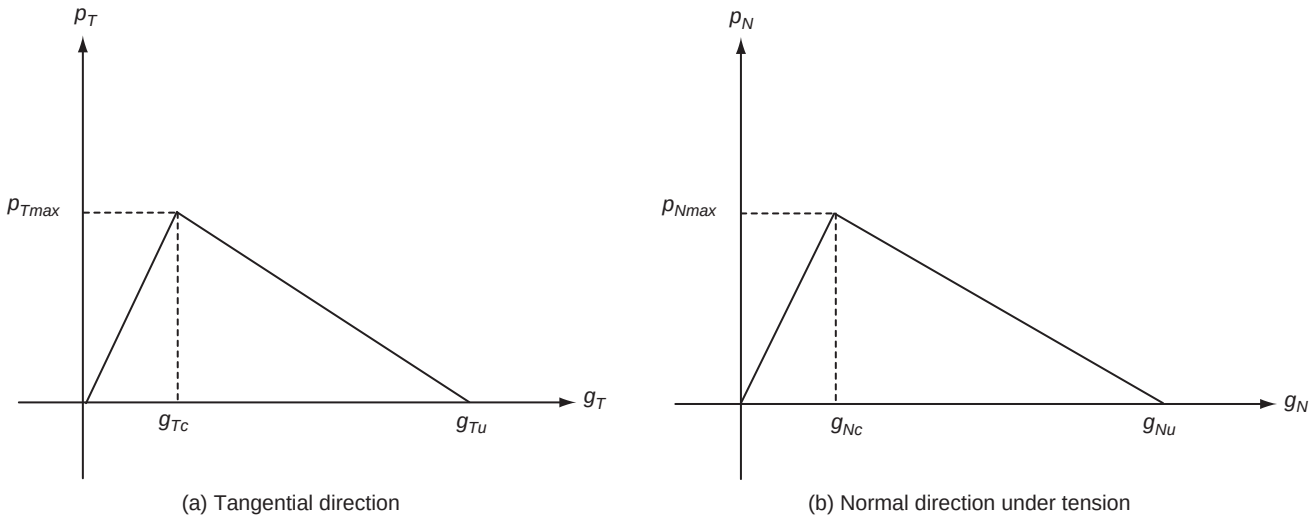

Figure 4. Interfacial cohesive laws

The normal and shear cohesive laws are coupled by introducing a measure of interface opening and sliding, λ, as follows (Tvergaard and Hutchinson 1992)

$$\lambda = \sqrt{\left(\frac{g_N}{g_{Nc}}\right)^2 + \left(\frac{g_T}{g_{Tc}}\right)^2} \tag{27}$$

where g_{Nc} and g_{Tc} are, respectively, the normal and shear relative displacements at peak traction. The normal and tangential tractions, F_N and F_T, are computed as functions of the normal and tangential relative displacements using the following relationships

$$F_N = \begin{cases} \left(\dfrac{p_{N\max}}{\lambda_{\max}}\right)\left(\dfrac{g_N}{g_{Nc}}\right) & 0 < \lambda \le \lambda_{\max} \\ \left(\dfrac{p_{N\max}}{\lambda}\right)\left(\dfrac{1-\lambda}{1-\lambda_{\max}}\right)\left(\dfrac{g_N}{g_{Nc}}\right) & \lambda_{\max} < \lambda < 1 \end{cases} \tag{28a}$$

$$F_T = \begin{cases} \left(\dfrac{p_{N\max}}{\lambda_{\max}}\right)\left(\dfrac{g_{Nc}}{g_{Tc}}\right)\left(\dfrac{g_T}{g_{Tc}}\right) & 0 < \lambda \le \lambda_{\max} \\ \left(\dfrac{p_{N\max}}{\lambda}\right)\left(\dfrac{1-\lambda}{1-\lambda_{\max}}\right)\left(\dfrac{g_{Nc}}{g_{Tc}}\right)\left(\dfrac{g_T}{g_{Tc}}\right) & \lambda_{\max} < \lambda < 1 \end{cases} \tag{28b}$$

Note that only one cohesive strength is explicitly defined ($p_{T\max} = p_{N\max}$), as the normal and tangential laws are derived from a potential. The curves vary with the coupling parameter λ. The parameter $\lambda_{\max}$ has no specific influence on the numerical results. The reason is that, in plate end debonding problems, Mode II is often largely prevalent and correspondingly there is very little influence of the Mode I contribution on results. In this study, $\lambda_{\max}$ is chosen sufficiently small as compared to the unity, to obtain a stiff ascending branch of the cohesive laws, which agrees with the experimental observations on the FRP-concrete interfacial behavior.

The crack-length control scheme is used in order to follow the whole range of the load-deflection behaviour of the plated beam, from the onset of debonding to the complete detachment of the plate. Such numerical scheme was proposed by Carpinteri (1985, 1989) for the analysis of the unstable mechanical response of quasi-brittle materials, and then extended in Carpinteri *et al.* (2005) to interface crack problems. Applications of this method to the problem of FRP debonding can be found in Carpinteri and Paggi (2008) and in Carpinteri and Paggi (2010).

6. NUMERICAL EXAMPLES

6.1. Rectilinear Beams

This example considers a beam characterized by the geometrical and mechanical parameters reported in Table 1. The analytically predicted dimensionless load-deflection curves are shown in Figure 5(a) for different values of k. The thick straight line corresponds to the load-deflection behaviour of the unplated beam. The curves feature both snap-back and snap-through instabilities, i.e. discontinuities appear if the process is either displacement- or load-controlled (Carpinteri and

Table 1. Parameters used in the numerical examples — rectilinear beams

Description	Parameter	Case 1	Case 2	Case 3
	Dimensional parameters			
Beam span	l [m]		1	
Cutoff distance	d [m]		0.125	
Beam depth	h [m]		0.12	
Beam width	b_c [m]		0.1	
Plate width	b_s [m]		0.1	
Beam elastic modulus	E_c [GPa]		30	
Plate elastic modulus	E_s [GPa]		210	
Plate thickness	t [m]	0.0015	0.0030	0.0045
Interface fracture energy	G_{cr} [N/m]		65	
	Dimensionless parameters			
Dimensionless cutoff distance	$\bar{d}$		0.125	
Dimensionless beam depth	$\bar{h}$		0.12	
Dimensionless plate width	$\bar{b}_s$		1	
Dimensionless plate thickness	$\bar{t}$	0.0125	0.0250	0.0375
Ratio of elastic moduli	n		7.0	
Ratio of bending stiffnesses	k	1.25	1.47	1.67
Dimensionless interface fracture energy	$\bar{G}_{cr}$		1.81E–8	

Paggi 2008; Carpinteri *et al.* 2007b). The predicted behaviour is thus very similar to that obtained by Carpinteri *et al.* (2007c) and Carpinteri and Paggi (2008, 2010) by finite element modelling and by Carpinteri *et al.* (2009a) using a one-parameter elastic foundation model for the plate-substrate interface. It is also worth noting that, for smaller values of the stiffness ratio k, the dimensionless critical load is higher, although the unstable snap-back branch is sharper.

The FE mesh is shown in Figure 3(a). The numerical predictions, always in terms of dimensionless load vs. dimensionless mid-span deflection, are reported in Figure 5(b). The parameters used in the cohesive zone laws are $G_{cr} = 65$ N/m, $p_{T\max} = p_{N\max} = 6$ MPa, $g_{Tc} = g_{Nc} = 2.2 \times 10^{-5}$ m and $\lambda_{\max} = 4.6 \times 10^{-3}$. With the exception of $\lambda_{\max}$, on which a comment was provided earlier, these values are thought to be realistic for FRP sheets bonded to concrete. The comparison between Figures 5(a) and 5(b) shows that the analytical model overestimates the critical (peak) load corresponding to the onset of FRP debonding, if compared to the FE solution. This agrees with previous results (Rabinovitch 2004), and is expectable, when considering the high degree of approximation involved in the analytical model. In particular, the analytical model does not incorporate the detailed distribution of interfacial stresses at the crack tip and the size of the fracture process zone. Conversely, these aspects are taken into account by the numerical model.

Concerning the experimental evidence of snap-back instability in rectilinear plated beams, the test results by Buyukozturk *et al.* (1998) can be used for a qualitative comparison with the previous analytical predictions. In such tests, beams with FRP strengthening plates of different lengths were considered. From a theoretical standpoint, this process is equivalent to adopting the interfacial crack length as the controlling parameter of the test. The experimental load vs. mid-span deflection curves are shown in Figure 6, where the different curves correspond to beams with different FRP lengths. As the figure clearly shows, the ideal curve joining the peaks of the various experimental load vs. mid-span deflection curves reproduces the snap-back profile predicted by the analytical model. Obviously, the pre-peak stage of the curve features a nonlinear behaviour which is not included in the model, since concrete is assumed to behave linear elastically.

6.2. Curved Beams

This example considers a beam characterized by the geometrical and mechanical parameters reported in Table 2. The analytically predicted dimensionless load vs. mid-span deflection curves are shown in Figure 7(a). The same considerations made for the rectilinear beam apply to this case.

The FE mesh is shown in Figure 3(b). For comparison, the numerical results obtained using the FE method for the same beams modelled analytically are shown in

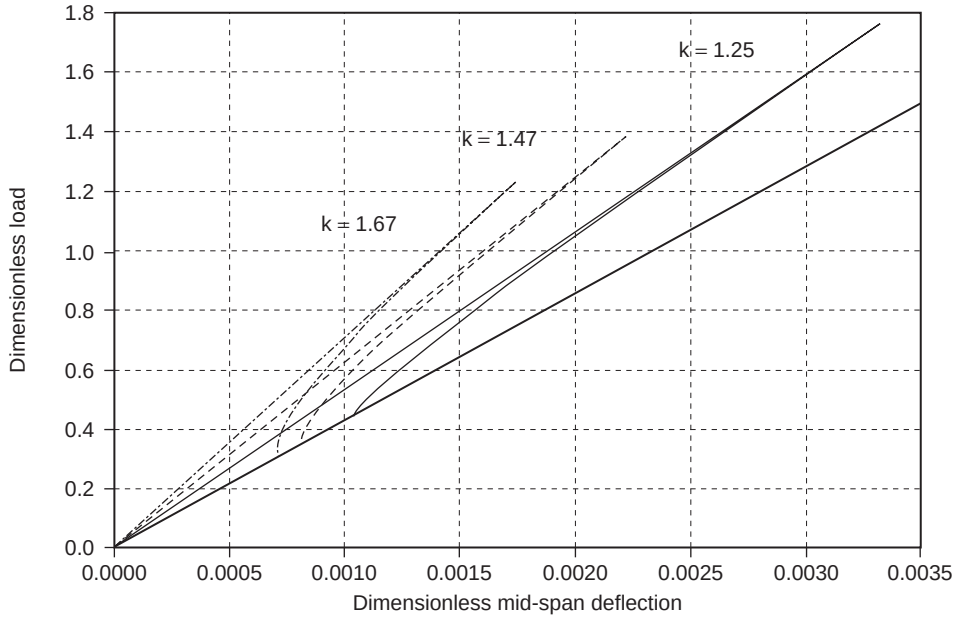

(a) Analytical predictions

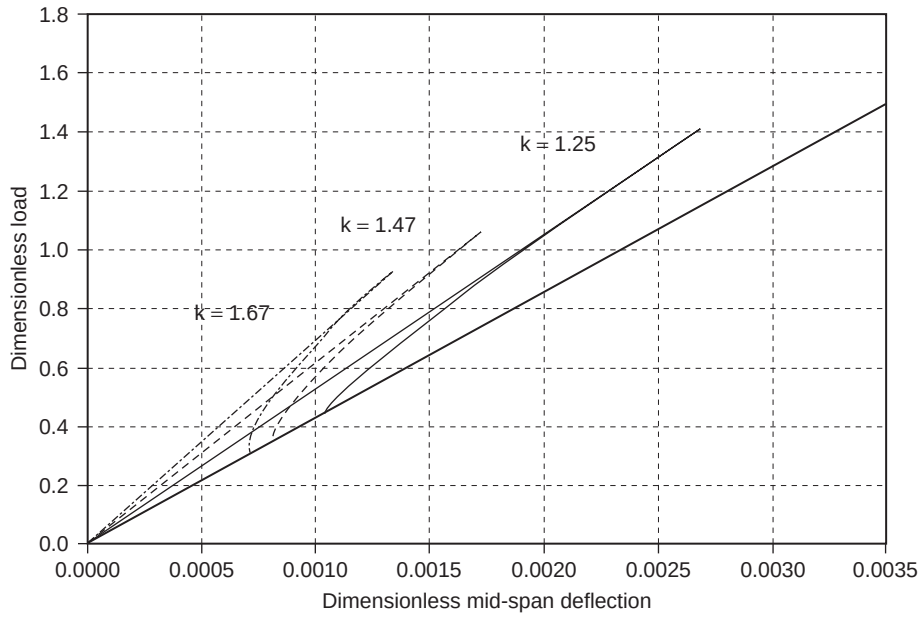

(b) Numerical predictions

Figure 5. Dimensionless load vs. mid-span deflection curves – rectilinear beams

Figure 7(b). These results are obtained by using the same interface parameters as for the rectilinear beams. Also in this case, the comparison between Figures 7(a) and 7(b) show that the analytical model overestimates the critical (peak) load corresponding to the onset of FRP debonding, if compared to the FE solution.

Figure 8 illustrates the variation of $F_{cr}(\alpha_d)$ with the dimensionless radius of curvature as predicted by the model based on linear elastic fracture mechanics. The dimensionless radius of curvature, $\bar{r}$, is varied from $\bar{r}_{\min} = (1 - \bar{h})/2 = 0.44$, corresponding to a semicircular beam, to $\bar{r}_{\max} \to \infty$, corresponding to a rectilinear beam. It is evident that, for values of $\bar{r}$ close to $\bar{r}_{\min}$, the critical load decreases very rapidly as the radius of curvature increases, and then stabilizes at a nearly constant value which corresponds to the critical load of the rectilinear beam. The $\bar{r}$ axis is truncated at a low value, beyond which no variation in the critical load is observed.

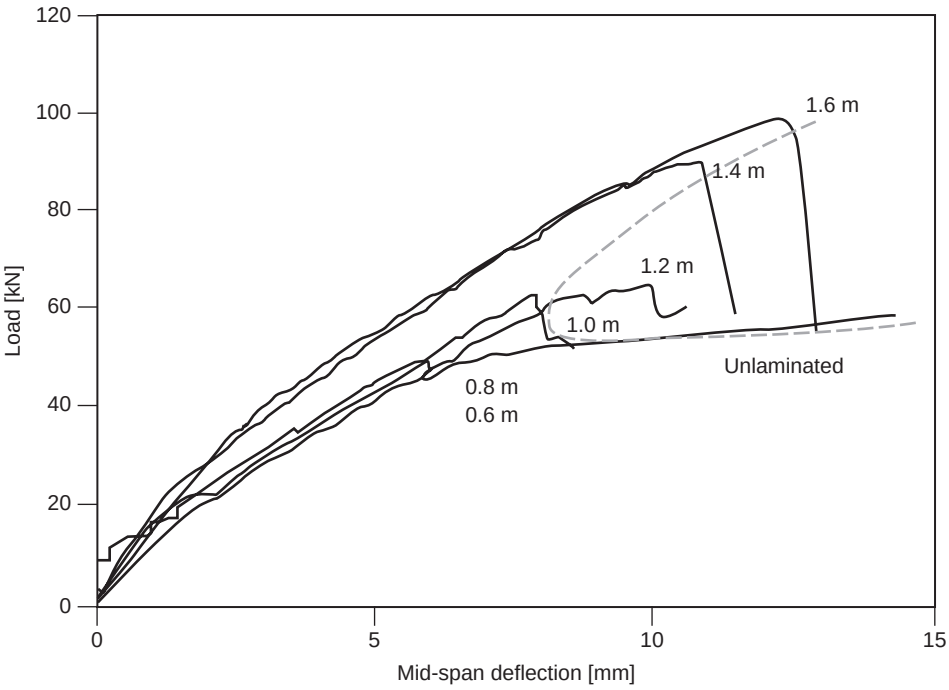

Figure 6. Experimental load vs. mid-span deflection curves for the beams tested by Buyukozturk *et al.* (1998)

Table 2. Parameters used in the numerical examples — curved beams

Description	Parameter	Case 1	Case 2	Case 3
		Dimensional parameters		
Beam span	l [m]		1	
Cutoff curvilinear distance	d_r [m]		0.125	
Beam depth	h [m]		0.12	
Beam width	b_c [m]		0.1	
Plate width	b_s [m]		0.1	
Beam elastic modulus	E_c [GPa]		30	
Plate elastic modulus	E_s [GPa]		210	
Plate thickness	t [m]		0.0030	
Interface fracture energy	G_{cr} [N/m]		65	
Radius of curvature	r [m]	0.44	0.45	∞
Cutoff curvilinear distance	Δx_d	0.078	0.100	0.125
		Dimensionless parameters		
Dimensionless cutoff curvilinear distance	$\bar{d}_r$		0.125	
Dimensionless beam depth	$\bar{h}$		0.12	
Dimensionless plate width	$\bar{b}_s$		1	
Dimensionless plate thickness	$\bar{t}$		0.0250	
Ratio of elastic moduli	n		7.0	
Ratio of bending stiffnesses	k		1.47	
Ratio of axial stiffnesses	k_A		1.175	
Dimensionless interface fracture energy	$\bar{G}_{cr}$		1.81E–8	
Dimensionless radius of curvature	$\bar{r}$	0.44	0.45	∞
Dimensionless cutoff curvilinear distance	$\overline{\Delta x_d}$	0.078	0.100	0.125

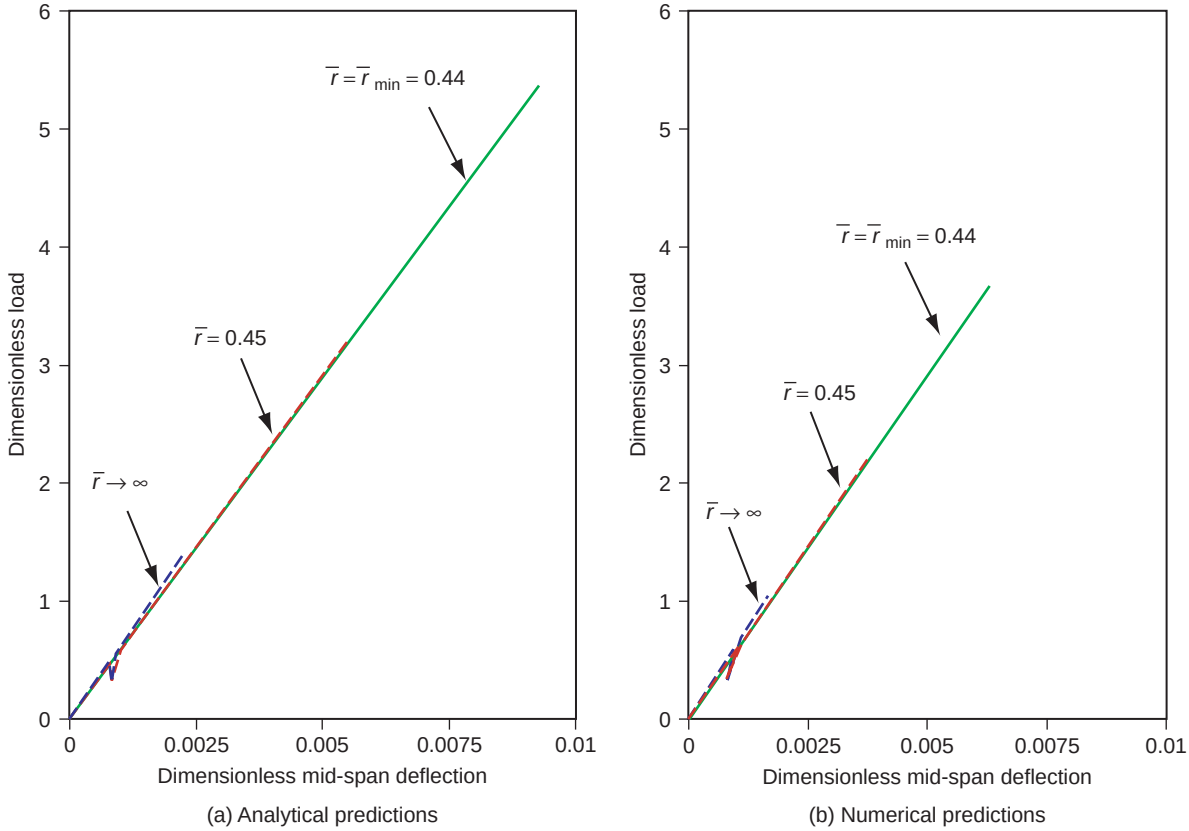

Figure 7. Dimensionless load vs. mid-span deflection curves – curved beams

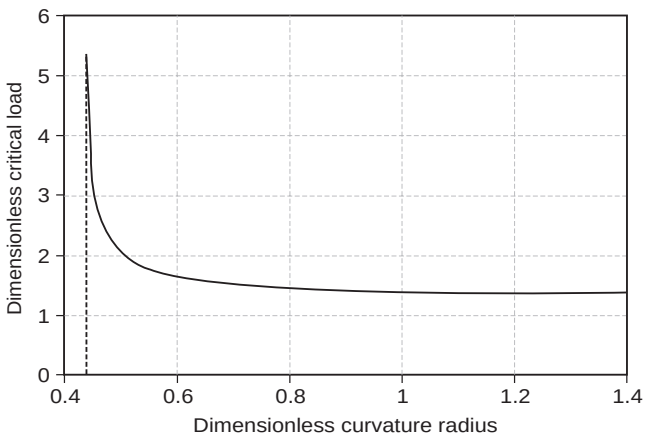

Figure 8. Effect of the curvature radius on the critical load

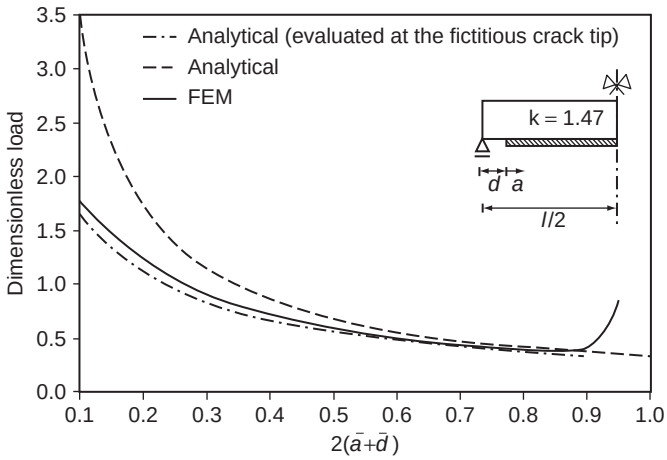

Figure 9. Dimensionless load vs. dimensionless interface crack length

7. IMPROVEMENT OF THE ANALYTICAL MODEL

In order to better interpret the discrepancy between analytical and numerical solutions, Figure 9 shows the dimensionless load vs. the relative length of the interfacial crack, $\bar{a}$, for a rectilinear plated beam. The diagram refers to the parameters corresponding to the case 2 in Table 1, but considers $\bar{d} = 0.05$ instead of $\bar{d} = 0.125$, in order to follow a broader range of the curve. Also in this plot the analytical curve is seen to overestimate the numerical predictions.

However, if the analytical model is applied by considering an increased fictitious crack length, $a + \Delta a$, instead of the real crack length a, the resulting analytical

curve matches closely the numerical one. The value of Δa corresponds to the length of the fracture process zone in front of the crack tip. Such a length can be estimated both analytically and numerically.

De Lorenzis and Zavarise (2009) proposed an analytical cohesive zone model for the determination of the shear stresses at the plate-beam interface. The model adopted a bilinear shape of the tangential cohesive zone law, with peak interfacial stress $p_{T\max}$, shear relative displacement at peak traction g_{Tc}, and ultimate shear relative displacement g_{Tu}. Defining the two further variables, $K = p_{T\max}/g_{Tc}$ and $k_\delta = g_{Tu}/g_{Tc}$, they found a closed-form expression for the length of the fracture process zone along the interface:

$$\Delta a = \frac{\sqrt{k_\delta - 1}}{\mu} \arctan\left(\sqrt{k_\delta - 1}\right) \tag{29}$$

where $$\mu = \sqrt{K\left[\frac{1}{E_s t} + \frac{4b_s}{E_c b_c h}\right]}.$$

For the case in Figure 9 (case 2 in Table 1), Eqn 29 provides $\Delta a = 0.05$ m. This size of the fracture process zone is in good agreement with that estimated from the interfacial stress distributions given by the FE model, which varies from 0.04 to 0.05 m during the debonding process. Adopting the correction provided by Eqn 29 in the analytical model, the dimensionless load vs. interface crack length becomes very close to that predicted by the FE solution (see the dashed-dotted line in Figure 9).

Following this approach, we also find that the parameter Δa estimated according to Eqn 29 is a slightly decreasing function of the plate thickness and, for the three case-studies reported in Table 1, it is equal to 0.04, 0.05 and 0.06 m, respectively. If the corresponding dimensionless load vs. dimensionless mid-span deflection curves are evaluated by using the incremented crack length $a + \Delta a$, a very close match between analytical and numerical results is achieved, the maximum deviation being about 4% (see Figure 10). Note that this approach shows analogies with the so-called "point method", widely used in the study of fatigue crack propagation, as well as with the effective crack approach used to account for small scale yielding in linear elastic fracture mechanics.

The analogous analytical-numerical comparison using the incremented crack length is shown in Figure 11 for the curved beams. Also in this case, the agreement between the analytical and the numerical solutions is significantly improved.

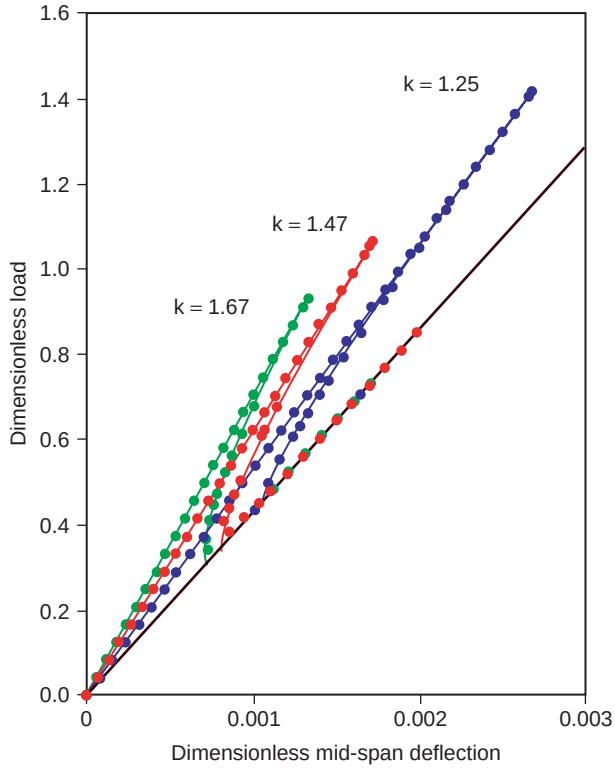

Figure 10. Numerical-analytical comparison for rectilinear beams (Solid curves = analytical solution using $a + \Delta a$, dots = FE solution)

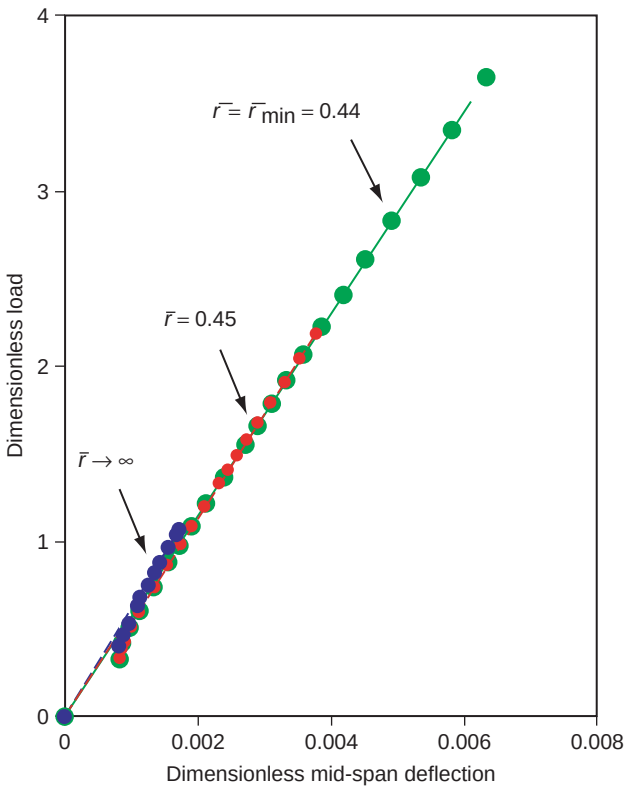

Figure 11. Numerical-analytical comparison for curved beams. Solid curves = analytical solution using $a + \Delta a$, dots = FE solution.

8. CONCLUSIONS

A linear elastic fracture mechanics approach for prediction of plate end debonding in rectilinear and curved plated beams has been presented in this paper. Closed-form equations have been provided, through which an approximate estimate of the critical load for the onset of plate end debonding can be obtained under the simplifying assumptions of the model. Moreover, the analysis has been extended to the determination of the entire load-deflection curve of the beam, obtained by controlling the length of the interfacial debonding crack. The shape of the curve shows that snap-back or snap-through instabilities may arise when the beam is loaded under displacement or force control. As the stiffness ratio between the plated and the unplated cross-sections decreases, the dimensionless critical load increases but the unstable snap-back branch becomes sharper. As the radius of curvature of the beam axis increases, starting from the minimum value corresponding to the semicircular beam, the critical load decreases very rapidly. It then stabilizes at a nearly constant value, which corresponds to the critical load of the rectilinear beam.

The analytical predictions have been compared with results of finite element modelling. It has been shown that the proposed analytical model significantly overestimates the critical load, due to its simplifying assumptions including infinite stiffness of the interfacial traction-separation law. However, if an effective crack length $a + \Delta a$ accounting for the size of the fracture process zone is used in the calculations, the resulting analytical predictions match closely the numerical solution. This approach shows analogies with the so-called "point method", widely used in the study of fatigue crack propagation, as well as with the effective crack approach used to account for small scale yielding in linear elastic fracture mechanics. It can be concluded that the proposed model with a modified crack length $a + \Delta a$, where Δa can be estimated in closed form from the cohesive zone parameters, provides a simple yet accurate prediction of the entire load-deflection response of plated rectilinear and curved beams.

REFERENCES

Anderson, T.L. (1994). *Fracture Mechanics: Fundamentals and Applications*, 2nd Edition, CRC Press.

Buyukozturk, O., Leung, C., Hearing, B. and Gunes, O. (1998). "Delamination criterion for concrete beams retrofitted with FRP laminates", *Fracture Mechanics of Concrete Structures*, H. Mihashi and K. Rokugo, eds., AEDIFICATIO Publishers, Freiburg, Germany, pp. 1771–1782.

Carpinteri, A. (1985). "Interpretation of the Griffith instability as a bifurcation of the global equilibrium", *Application of Fracture Mechanics to Cementitious Composites,* S. Shah, ed., Evanston, USA.

Carpinteri, A. (1989). "Cusp catastrophe interpretation of fracture instability", *Journal of the Mechanics and Physics of Solids*, Vol. 37, No. 5, pp. 567–582.

Carpinteri, A., Cornetti, P. and Pugno, N. (2007a). "Debonding in FRP strengthened beams: stress assessment versus fracture mechanics approach", *Proceedings of the 6th Conference on Fracture Mechanics of Concrete and Concrete Structures (FraMCoS)*, Catania, Italy, pp. 1053–1060.

Carpinteri, A., Lacidogna, G. and Paggi, M. (2007b). "On the competition between delamination and shear failure in retrofitted concrete beams and related scale effects", *Proceedings of the 6th Conference on Fracture Mechanics of Concrete and Concrete Structures (FraMCoS)*, Catania, Italy, pp. 1069–1076.

Carpinteri, A., Lacidogna, G. and Paggi, M. (2007c). "Acoustic emission monitoring and numerical modelling of FRP delamination in RC beams with non-rectangular cross-section", *Materials & Structures*, Vol. 40, No. 6, PP. 553–566.

Carpinteri, A., Cornetti, P., Lacidogna, G. and Paggi, M. (2009a). "Towards a unified approach for the analysis of failure modes in FRP-retrofitted concrete beams", *Advances in Structural Engineering*, Vol. 12, No. 5, pp. 715–729.

Carpinteri, A., Cornetti, P. and Pugno, N. (2009b). "Edge debonding in FRP strengthened beams: Stress versus energy failure criteria", *Engineering Structures*, Vol. 31, No. 10, pp. 2436–2447.

Carpinteri, A. and Paggi, M. (2010). "Analysis of snap-back instability due to end-plate debonding in strengthened beams", *Journal of Engineering Mechanics*, ASCE, Vol. 136, No. 2, pp. 199–208.

Carpinteri, A. and Paggi, M. (2008). "A crack-length control scheme for the analysis of snap-back instability in the delamination of strengthened beams", *Proceedings of the 8th World Congress on Computational Mechanics (WCCM8) and 5th European Congress on Computational Methods in Applied Sciences and Engineering (ECCOMAS 2008)*, Venice, Italy.

Carpinteri, A., Paggi, M. and Zavarise, G. (2005). "Snap-back instability in micro-structured composites and its connection with superplasticity", *Strength, Fracture and Complexity*, Vol. 3, No. 2-4, pp. 61–72.

Colombi, P. (2006). "Reinforcement delamination of metallic beams strengthened by FRP strips: fracture mechanics based approach", *Engineering Fracture Mechanics*, Vol. 73, No. 14, pp. 1980–1995.

Cornetti, P., Puzzi, S. and Carpinteri, A. (2007). "Failure mechanisms in beams strengthened with adhesive strips", *Proceedings of the XVIII AIMETA Conference*, Brescia, Italy.

De Lorenzis, L. and Zavarise, G. (2008). "Modeling of mixed-mode debonding in the peel test applied to superficial reinforcements", *International Journal of Solids and Structures*, Vol. 45, No. 20, pp. 5419–5436.

De Lorenzis, L. and Zavarise, G. (2009). "Cohesive zone modelling of interfacial stresses in plated beams", *International Journal of Solids and Structures*, Vol. 46, No. 24, pp. 4181–4191.

Paggi, M., Carpinteri, A. and Zavarise, G. (2006). "A unified interface constitutive law for the study of fracture and contact problems in heterogeneous materials", *Analysis and Simulation of Contact Problems*, P. Wriggers and U. Nackenhorst, eds., Springer-Verlag, Berlin, pp. 297–304.

Rabinovitch, O. (2004). "Fracture-mechanics failure criteria for RC beams strengthened with FRP strips – a simplified approach", *Composite Structures*, Vol. 64, No. 3-4, pp. 479–492.

Rabinovitch, O. and Frostig, Y. (2001). "Non-linear high-order analysis of cracked RC beams externally strengthened with FRP strips", *Journal of Structural Engineering*, ASCE, Vol. 127, No. 4, pp. 381–389.

Smith, S. and Teng, J.G. (2002). "FRP-strengthened RC beams. I: review of debonding strength models", *Engineering Structures*, Vol. 24, No. 4, pp. 385–395.

Timoshenko, S. and Young, D.H. (1965). *Theory of Structures*, 2nd Edition, McGraw-Hill Book Company.

Tvergaard, V. (1990). "Effect of fiber debonding in a whisker-reinforced metal", *Materials Science and Engineering* A, Vol. 125, No. 2, pp. 203–213.

Tvergaard, V. and Hutchinson, J.W. (1992). "The relation between crack growth resistance and fracture process parameters in elastic-plastic solids", *Journal of the Mechanics and Physics of Solids*, Vol. 40, No. 6, pp. 1377–1397.

Yuan, H., Teng, J.G., Seracino, R., Wu, Z.S. and Yao, J. (2004). "Full-range behaviour of FRP-to-concrete bonded joints", *Engineering Structures*, Vol. 26, No. 5, pp. 553–565.

NOTATION

$\bar{a} = \dfrac{a}{l}$	dimensionless crack length
$\bar{d} = \dfrac{d}{l}$	dimensionless distance between the support and the cutoff section of the strengthening plate
$\bar{h} = \dfrac{h}{l}$	dimensionless beam depth
$\bar{b}_s = \dfrac{b_s}{b_c}$	dimensionless plate width
$\bar{t} = \dfrac{t}{h}$	dimensionless plate thickness
$\bar{r} = \dfrac{r}{l}$	dimensionless radius of curvature
$k = \dfrac{EI_s}{EI_u}$	bending stiffness ratio between plated and unplated cross-sections
$k_A = \dfrac{EA_s}{EA_u}$	axial stiffness ratio between plated and unplated cross-sections
$n = \dfrac{E_s}{E_c}$	modular ratio between plate and beam materials
$\bar{G}_{cr} = \dfrac{G_{cr}}{Eh}$	dimensionless mode II fracture energy
$\bar{F}_{cr} = \dfrac{F_{cr}}{b_s\sqrt{EG_{cr}h}}$	dimensionless critical force
$\bar{v} = \dfrac{v}{l}$	dimensionless mid-span deflection
$\bar{C} = C\dfrac{b_s\sqrt{EG_{cr}h}}{l}$	dimensionless compliance